land

Article

Potential Variation of Evapotranspiration Induced by Typical Vegetation Changes in Northwest China

Yanmin Shuai [1,2,3,4], Yanjun Tian [2,*], Congying Shao [1,2], Jiapeng Huang [2], Lingxiao Gu [5], Qingling Zhang [6] and Ruishan Zhao [2]

[1] Xinjiang Institute of Ecology and Geography, Chinese Academy of Sciences, Urumqi 830011, China; shuaiym@ms.xjb.ac.cn (Y.S.); 471910037@stu.lntu.edu.cn (C.S.)
[2] School of Geomatics, Liaoning Technical University, Fuxin 123000, China; huangjiapeng@lntu.edu.cn (J.H.); zhaoruishan@lntu.edu.cn (R.Z.)
[3] Research Center for Ecology and Environment of Central Asia, Chinese Academy of Sciences, Urumqi 830011, China
[4] College of Resources and Environmental, University of Chinese Academy of Sciences, Beijing 100049, China
[5] School of Surveying and Land Information Engineering, Henan Polytechnic University, Jiaozuo 454003, China; 471810033@lntu.edu.cn
[6] School of Aeronautics and Astronautics, Sun Yat-sen University Shenzhen Campus, Shenzhen 518107, China; zhangqling@mail.sysu.edu.cn
* Correspondence: 471920552@stu.lntu.edu.cn

Abstract: Evapotranspiration (ET), as a key eco-hydrological parameter, plays an important role in understanding sustainable ecosystem development. Each plant category has a unique functional trait on transpiration and photosynthesis, with ET implying that water cycle and energy transformation is linked with vegetation type. Changes in surface vegetation directly alter biophysical land surface properties, hence affecting energy and ET transfer. With the rapid increase in land surface changes, there is a need to further understand and quantify the effects of vegetation change on ET, especially over the vulnerable water-cycle region in the arid and semi-arid regions of Northwest China. We adopted the GlobalLand30 land cover and MOD16A2 in 2010 and 2020 to investigate, discuss the spatio-temporal characteristics of annual and seasonal ET of cultivated land, grassland, and forests in Northwest China, and quantify the impact on vegetation changes with absolute and relative changes from different climatic subecoregions on ET. Our results show the following: (1) Forest ET was generally the highest at 688 mm, followed by cultivated land and grassland with 200–400 mm in arid climatic subecoregions. (2) Returning cultivated land to forests and cultivated land expansion potentially enhances ET by 90–110 mm/10a, with the relative rate of change increasing by 22.1% and 45.8%, respectively, away from unchanged vegetation within identical subecoregions. (3) The ET of most investigated areas gains the highest value in summer, followed by spring, autumn, and winter. This study provides reference for sustainable ecosystem development and the reasonable utilization of limited water resources in Northwest China.

Keywords: evapotranspiration; vegetation change; water resources; variation; Northwest China

Citation: Shuai, Y.; Tian, Y.; Shao, C.; Huang, J.; Gu, L.; Zhang, Q.; Zhao, R. Potential Variation of Evapotranspiration Induced by Typical Vegetation Changes in Northwest China. *Land* **2022**, *11*, 808. https://doi.org/10.3390/land11060808

Academic Editors: Ilan Stavi and Dailiang Peng

Received: 25 March 2022
Accepted: 19 May 2022
Published: 30 May 2022

1. Introduction

Evapotranspiration (ET) is defined as the transpiration of vegetation, and evaporation from vegetation surfaces, soil, and water [1]. It is a crucial bond of soil–vegetation–atmosphere interactions, and is a key link of surface energy carbon and water cycles [2]. ET plays an important role in the process of energy distribution, and determines the distribution of latent and sensible heat fluxes [3–5]. In a water cycle, approximately 60% of precipitation is returned to the atmosphere in the form of ET, and a larger proportion of water resources is returned to the atmosphere in arid and semi-arid regions with intense ET capacity. Precipitation and ET greatly determine the growth and even survival of vegetation [6]. Carbon dioxide concentrations have continued to rise in recent years, which causes global warming and could then exacerbate ET, and above-ground biomass is key to regional carbon and water cycles [7–9]. In most countries, carbon neutrality is achieved by expanding the area of forests to absorb carbon dioxide [10–12]. This improves the water vapor content in the atmosphere and increases global precipitation, thus promoting the water cycle. Therefore, the quantitative description of surface ET is greatly significant for global energy, carbon, and water cycles.

The ET model was studied from the perspective of interaction processes and mechanisms. With the rapid development of remote-sensing technologies, ET products at the regional or global scale are gradually becoming possible, which has attracted the attention of researchers. This has achieved some progress with inversion methods and products of satellite-based ET. Data-driven empirical regression, machine-learning, and data-fusion methods were used to invert ET products [13]. Different researchers and institutions published ET-related data products, including global products, such as MOD16A2 [13–16], GLASS [17] and MPI [18], and regional ET products such as those of the Heihe River Basin [19,20], the Northern China and Haihe River Basin [20]. One of the most widely used is global terrestrial ET product MOD16A2, jointly released by the United States National Aeronautics and Space Administration (NASA) and the University of Montana Numerical Terradynamic Simulation Group (NTSG). He et al. [21] analyzed the spatio-temporal variation characteristics of ET in China on the basis of MOD16A2. Thus, there is the opportunity to quantitatively analyze ET.

Many ET products provide opportunities for studying ET, but land cover is one of the most important factors to determine the magnitude of ET. In Northwest China, in order to improve the ecological environment, and prevent desertification in arid and semi-arid regions, the Chinese government launched ecological programs, such as the Great Green Wall Program (1978–present), Grain for Green Program (1999–present), Grassland Ecological Protection Program (2000–present), and Beijing–Tianjin Sandstorm Source Control Project (2002–present). These programs have greatly contributed to revegetation in arid and semi-arid regions, for example, cultivated land was converted into forest in the Loess Plateau of Northwest China [22]. The policy of cultivated land protection plays an important role in maintaining the balance of total cultivated land and solving the problem of Chinese food security. The center of new increased cultivated land moved to Northwest China [23,24]. In short, vegetation has significantly changed in Northwest China in the past decade, which in turn affects ET.

In recent years, the response from ET has achieved progress in land cover changes. Previous studies explored the responses of ET to land cover changes in typical regions, such as the Heihe River Basin and Loess Plateau. Land cover changes affected the water balance, including the impact on precipitation, ET, and runoff, and ET decreased after the conversion of grass into bare land in the Heihe River Basin [25]. Water consumed in crop expansion in the Heihe River Basin could be used to recover nearly ten times as much as the area of the degraded desert grassland ecosystem [26], and this increased ET largely intensified the water crisis in Northwest China. Vegetation restoration plays an important role in regulating water resources; the Loess Plateau is an important revegetation area [27,28]. Vegetation restoration has led to a significant reduction in land surface albedo, increased radiative forcing, and increased ET [29], and the cooling effect of ET counteracts the warming effect of albedo and alleviates the trend of global warming to some extent [30–32]. Thus, several studies have focused on the ET response to vegetation changes in Northwest China in the past ten years.

Due to differences in the physiological processes of different vegetation types, changes in vegetation had a certain influence on ET in Northwest China. Water resources are scarce in Northwest China, and water is the main limiting factor of vegetation growth that could then affect ET. Vegetation growth had obvious seasonal differences [33,34]. It is still insufficient to quantitatively describe inter-annual and seasonal variations in ET values after vegetation changes in Northwest China. Considering the spatio-temporal resolution and the coverage of ET products, we selected the MOD16A2 product to better capture seasonal

ET changes. We investigated the ET characteristics of the typical vegetation of grassland, cultivated land, and forests, and the effects of vegetation changes on inter-annual and seasonal ET in different subecoregions of Northwest China. This can provide reference for the carbon balance [35], and in response to climate change and water-resource management. It is greatly significant to the sustainable development of ecological environment protection.

2. Materials and Methods

2.1. Study Area

Northwest China is a typical arid and semi-arid region with sandy soil in China. The average annual precipitation is below 350 mm, with a large temperature difference between day and night, and long days of sunshine, which is conducive to the accumulation of photosynthetic substances in vegetation and accompanied by a large amount of water returning to the atmosphere in the form of ET. Northwest China administratively comprises Xinjiang, Gansu, Qinghai, Ningxia, and Shaanxi (Figure 1, review no. GS(2019)1822).

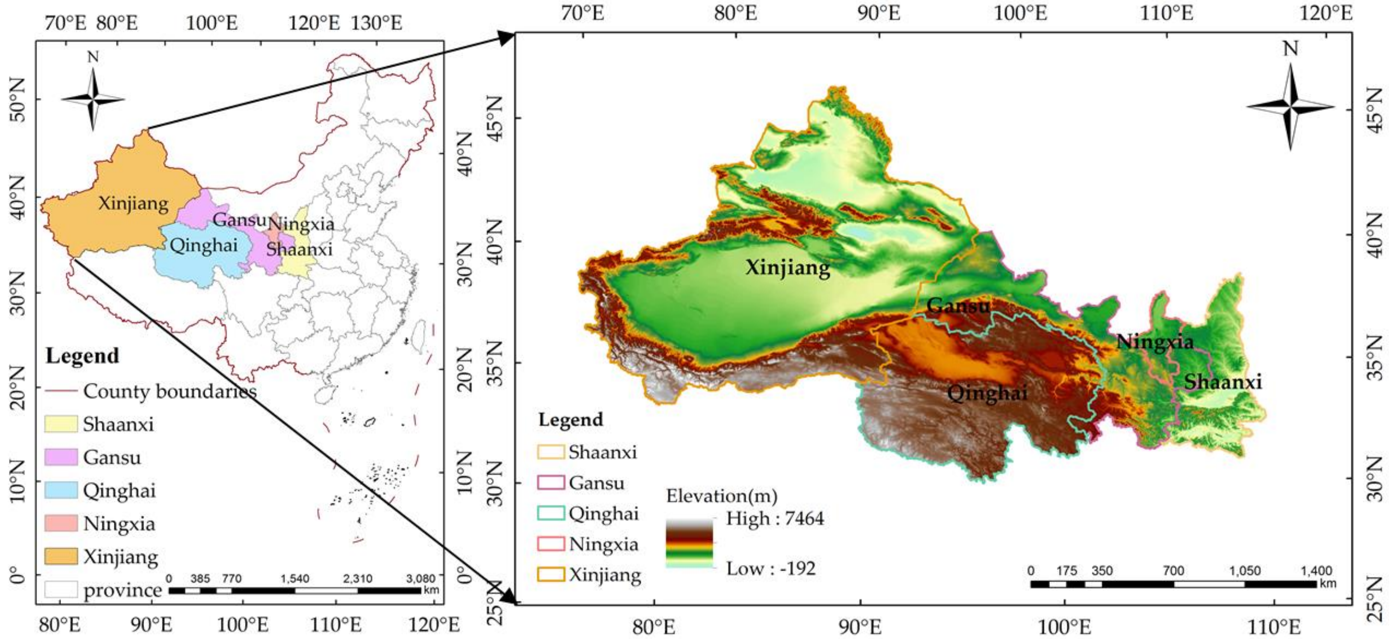

Figure 1. Study area of Northwest China.

There are alternate basins with the Xinjiang mountains, with oasis agriculture scattered between the mountains and basins. The Altai Mountains are located in the north of Xinjiang, the Tianshan Mountains are located in the middle of Xinjiang, and the Kunlun Mountains are located in the south of Xinjiang. The Junggar and Tarim basins are between the mountains, with the characteristics of three mountains sandwiched between two basins. Benefiting from mountain glacier and snow melting, Xinjiang has formed a unique agricultural oasis climate area in Northwest China. The topography of Gansu is complex and diverse, with mountains, plateaus, plains, valleys, and the Gobi Desert. The Hexi Corridor is the famous Gobi agricultural oasis development region. Agricultural irrigation is required in Xinjiang and Gansu. Qinghai is the birthplace of China's three major rivers, the Yangtze, Yellow, and Lancang Rivers, and plays an important role in hydro-ecology in China; a variety of drought- and cold-resistant grasses grow in Qinghai. The south of Ningxia is dominated by flowing water erosion, while the northern part is dominated by droughts, and mountains, hills, and alluvial plains formed by the Yellow River. Shaanxi is the main part of the Loess Plateau, which is a typical vegetation ecological restoration area, and the key area of afforestation and re-turning cultivated land to forest and grassland since the beginning of the 21st century.

2.2. Study Data

2.2.1. Land Cover and Preprocessing

In this study, we used a global land cover dataset product (GlobalLand30) with a spatial resolution of 30 m [36–38]; inputs for GlobalLand30 are mainly 30 m multispectral images, including multispectral images of the Landsat and the Chinese Environmental Disaster Alleviation Satellite (HJ-1). This developed three phases of data for 2000, 2010, and 2020 on the basis of the method of hierarchical extraction. The spatial resolution of GlobalLand30 is 30 × 30 m, including cultivated land, forest, grassland, shrub-land, wetland, water bodies, tundra, artificial surfaces, bare land, permanent snow, and ice. "Cultivated land" is defined as land used, for example, for agriculture, horticulture, and gardens, including paddy fields, irrigated and dry cultivated land vegetation, and fruit gardens. "Forest" is defined as land covered with trees, with vegetation cover over 30%, including deciduous and needle leaf forests, and sparse woodland with 10–30% cover. "Grassland" is defined as land covered by natural grass with cover over 10%. Classification accuracy for cultivated land, forests, and grassland was 83.06%, 88.99% and 76.85%, respectively.

Considering all available data, we downloaded the 2010 and 2020 datasets from the Global Geographic Information Public Product (http://www.globeland30.org/, accessed on 30 December 2020). By manual visual interpretation comparison with high-resolution Google Earth images, the classification of land cover was accurate. We mainly analyzed changes in cultivated land, forests, and grassland in the past ten years.

2.2.2. Evapotranspiration and Preprocessing

Global terrestrial ET product MOD16A2 was produced by NASA in 2011. The MOD16A2 algorithm is based on the Penman–Monteith equation (see Equation (1)), which used daily meteorological reanalysis dataset GMAO or MERRA GMAO, MCD43B2/MCD43B3, and MOD15 A2 (FPAR/LAI). The 8-day MOD16A2 was validated with ET measured at eddy flux towers; the correlation coefficient was approximately 0.85 [13–16]. The MOD16A2 algorithm takes into account soil surface evaporation, canopy interception, and water evaporation and vegetation, and reflects the heterogeneity of deserts and oases underlying surface wells. The MOD16A2 product contains 8 days of the dataset at 500 m spatial resolution.

$$LE = \frac{\Delta \times (R_n - G) + \rho \times C_p \times (e_{sat} - e)/r_a}{\Delta + \gamma \times (1 + r_s/r_a)} \tag{1}$$

where R_n represents the net surface radiation flux (w·m^{-2}); G represents the soil heat flux (w·m^{-2}); Δ is the slope of the saturated vapor pressure–temperature curve; ρ represents air density (kg·m^{-3}); C_p represents constant pressure heat ratio of air (J·kg^{-1}K^{-1}); e_{sat} represents the surface saturated vapor pressure (Pa); e represents atmospheric vapor pressure (Pa); γ represents dry and wet bulb constants; r_{a} represents the resistance of evaporation surface to air transmission (s m^{-1}); r_{s} represents all resistance to evaporation of the vegetation canopy, soil, and other underlying surfaces (s·m^{-1}).

We used the MOD16A2 product of 2010 and 2020, with tiles h23v05, h24v04, h24v05, h25v04, h25v05, h26v05 and h27v05 (https://ladsweb.modaps.eosdis.nasa.gov/, accessed on 31 January 2021). The ET datasets were used to select pixels with good quality according to the corresponding quality-control files for statistical analysis. In this paper, temporal latent heat flux (LE) observations from the Haibei site of China Flux in 2010 were used to verify the applicability of MOD16A2 in Northwest China [21]. Because the temporal resolution of China Flux is daily and in MW/m^2, while the temporal resolution of MOD16A2 is per 8 days in J/m^2, we converted them into the 8-day format in MW/m^2 and performed correlation analysis using the R^2 determinant. The specific calculation formula is as follows. Scatterplots of latent heat (Figure 2) indicated good correlations (R^2 = 0.781) between the simulations and observations, and the root mean square error (RMSE) of LE was around

1.76 MW/m^2/8-day; PBIAS showed that the MOD16A2 value was a little overestimated (Table 1). This indicated that the product has confidence when applied to Northwest China.

$$R^2 = 1 - \frac{\sum_{i=1}^{n}\left(LE^{CF} - LE^{MOD}\right)^2}{\sum_{i=1}^{n}\left(LE^{CF} - \overline{LE}^{CF}\right)^2} \tag{2}$$

$$RMSE = \sqrt{\frac{\sum_{i=1}^{n}\left(LE^{CF} - LE^{MOD}\right)^2}{n}} \tag{3}$$

$$PBIAS = \frac{\sum_{i=1}^{n}\left(LE^{CF} - LE^{MOD}\right) * 100}{\sum_{i=1}^{n}\left(LE^{CF}\right)} \tag{4}$$

where LE^{CF} represents the value of China Flux LE, and LE^{MOD} represents the value of MOD16A2 LE.

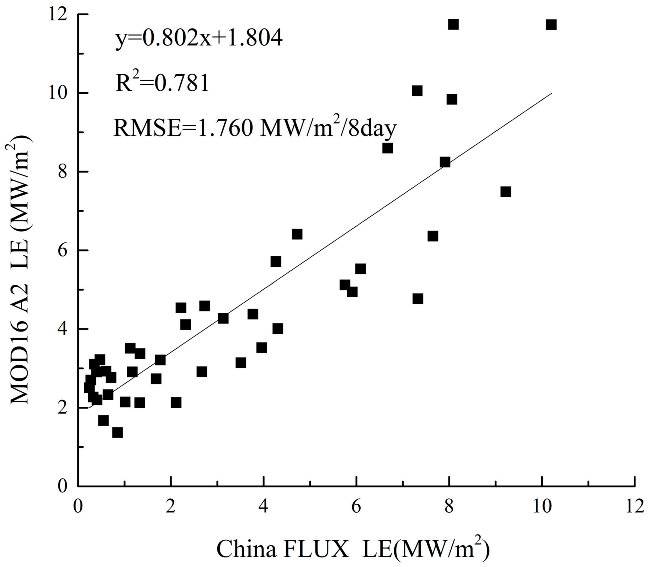

Figure 2. Validation of MOD16A2 latent heat flux.

Table 1. Validation of MOD16A2 latent heat flux.

DOY	PBIAS	DOY	PBIAS
49	−59.727	201	−14.965
57	−211.321	209	−45.015
65	−148.666	217	−37.461
73	−81.076	225	−4.127
81	−0.670	233	18.862
89	−77.009	241	9.271
97	−67.892	249	34.974
105	−36.304	257	−35.628
113	11.057	265	−104.327
121	10.660	273	−9.032
129	−16.079	281	−62.236
137	7.009	289	−152.270

Table 1. *Cont.*

DOY	PBIAS	DOY	PBIAS
145	−33.835	305	−110.994
153	11.063	313	−384.156
161	16.419	321	−621.961
169	16.888	345	−592.443
185	−28.735	353	−436.365
193	−21.970	361	−204.055

2.2.3. Subecoregion Vector

Northwest China is a vast region with different climatic and geographic conditions, and many vegetation categories. There is interaction between climate and topography [39–43], and the ET of vegetation varies dramatically in different subecoregions. Therefore, we relied on ecoregional data provided by the Database of Ecological Function Region in China to exclude the impact of climatic conditions on ET as much as possible (http://www.ecosystem.csdb.cn/ecoass/ecoecoplanning.jsp/, accessed on 18 March 2021). We discuss vegetation changes regions in Northwest China by regionalization. On the basis of the area of vegetation changes, we selected subecoregional data to divide typical change areas in Northwest China. Table 2 shows the nine subecoregions with major changes, and their spatial distribution is presented in Figure 3 (review no. GS (2019)1822).

Table 2. Subecoregion data.

Code	Name	Geographic Location
I1204	Cultivated land and grassland subecoloregion of Loess hilly remnant tableland in southeast Gansu.	The subecoregion is located in the southern part of the Ningxia Hui Autonomous Region and the eastern part of Gansu province.
I1207	Western agricultural subecoregion of Loess Plateau.	The subecoregion is located in the west of the Loess Plateau, the Loess hilly region in the middle of Gansu province, the Hulu River valley in the southwest of Ningxia, and the Liangmao hills on both sides.
I1501	Subecoregion of deciduous broad-leaf conifer and broadleaf mixed forests in Qinling Mountains.	The subecoregion is located in the Qinling mountains, across Gansu, Shaanxi, and Henan provinces.
II0303	Arid desert oasis agricultural subecoregion in Hexi Corridor.	The subecoregion is located in the eastern section of the Hexi Corridor in Gansu province.
II0604	Desert, and shrubby and semishrubby oasis agricultural subecoregion in southern Junggar Basin.	The subecoregion is located in the south and southeast of Junggar Basin. The piedmont plain of the northern foot of the Tianshan Mountain reaches the foot of the Tianshan Mountain in the south, the southern boundary of the Goulban Tungut Desert in the north, the western boundary of the city of Wusu in the west, and the Baitou township of Autonomous County Muleh Kazakh in the east.
II0702	Desert steppe–oasis agricultural subecoregion on the southern slope of Tianshan Mountains.	The subecoregion is located in western and central Xinjiang.
II0803	Desert oasis agricultural subecoregion in northern Tarim Basin.	The subecoregion is located in the northern part of Tarim Basin, Tianshan piedmont plain, Kashgar Delta and Tarim River alluvial plain.
III0401	Alpine grassland subecoregion in Gonghe Basin.	The subecoregion is located in the Gonghe Basin south of Qinghai Lake.
III0405	Alpine meadow grassland subecoregion of Lancang River source.	The subecoregion is located in the southern most part of Autonomous Prefecture Qinghai Yushu Tibet.

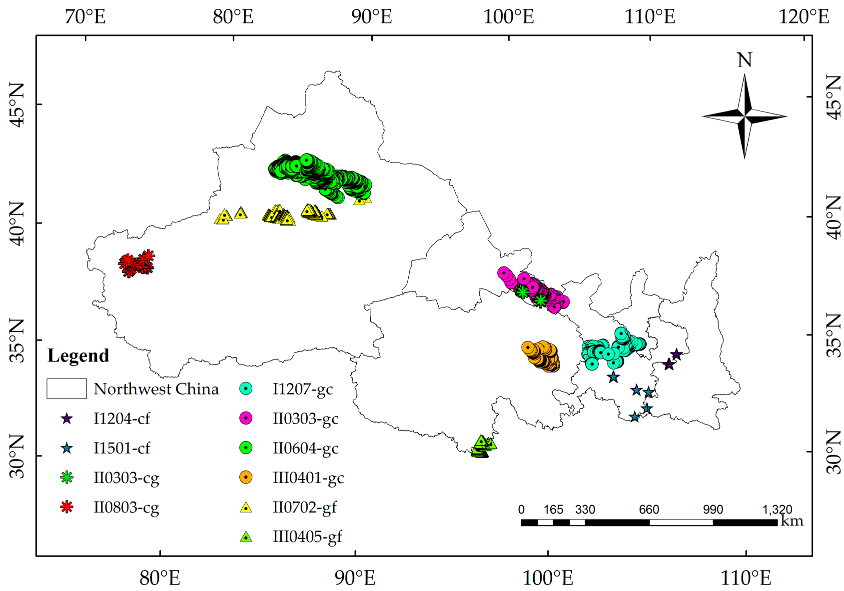

Figure 3. Spatial distribution of the selected site in subecoregions in Northwest China.

2.2.4. NDVI and Preprocessing

We discuss the effect of vegetation changes on ET, and vegetation changes usually occurred in boundary zones of vegetation. The distribution of vegetation is more complex in Northwest China, with forests, grassland, and cultivated land being alternately distributed. Therefore, to ensure the accuracy of the pixels that we selected, we further improved the accuracy of cultivated land, forests, and grassland by extracting MOD13A1 time series data [44]. MOD13 A1 is produced by NASA (https://ladsweb.modaps.eosdis.nasa.gov/, accessed on 26 May 2021). The MOD13 A1 product contains 16 days of data at 500 m spatial resolution with tiles h23v05, h24v04, h24v05, h25v04, h25v05, h26v05 and h27v05.

The composition proportion and organizational structure of the canopy groups had obvious seasonal characteristics of cultivated land, forest, and grassland, and they showed different characteristics in the Normalized Difference Vegetation Index (NDVI) [45]; ET of the same vegetation type in different subecoregions also shows differences. In this paper, we established a standard rule for distinguishing cultivated land, forest, and grassland by using the NDVI. Forest was the highest, followed by cultivated land and grassland. The cultivated land, forest, and grassland indices are shown in Figure 4.

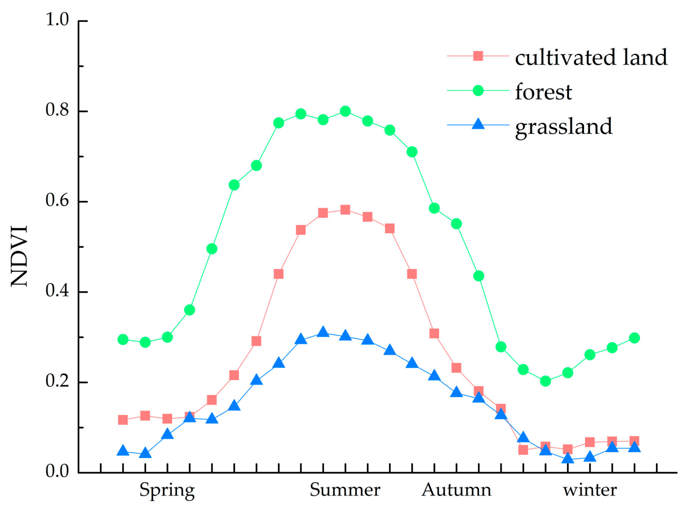

Figure 4. Temporal features in typical vegetation.

2.3. Methods

This flowchart of this study is shown in Figure 5. First, vegetation information in Northwest China was extracted from Global Land30 data in 2010 and 2020, and vegetation changes could be obtained via transfer matrix. Climatic, topographic, and vegetation characteristics were more complex in different regions in Northwest China. Thus, we discuss vegetation changes in Northwest China on the basis of the subecoregion. Then, vegetation growth presented by temporal MOD13 A1 was used for the auxiliary verification of extracted vegetation-change pixels to further improve the accuracy of cultivated land, forest, and grassland. Lastly, ET corresponding to vegetation-change areas were extracted on the basis of relatively accurate pixels. The influence of typical vegetation changes on ET was analyzed regarding inter-annual and seasonal variation.

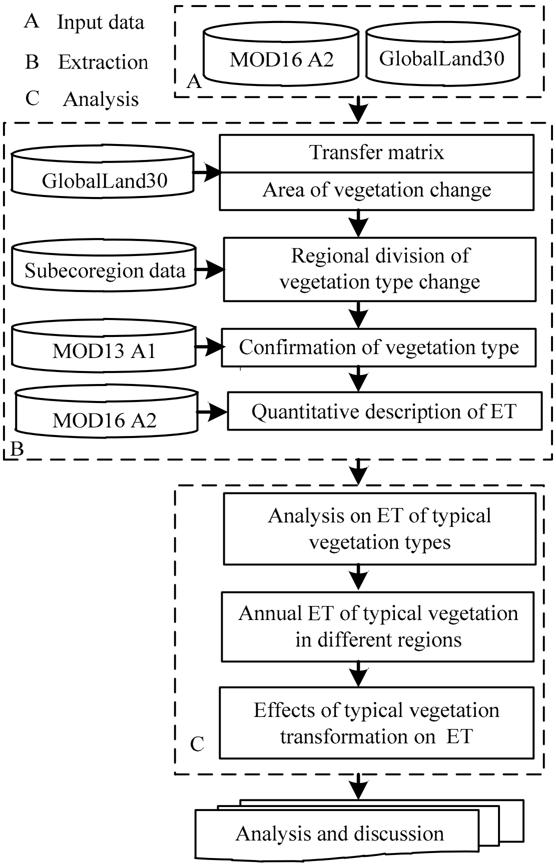

Figure 5. Flow-chart of information process.

2.3.1. Land Cover Transfer Matrix

The land cover transfer matrix reflects the situation and direction of mutual transformation between different land cover types in the research period [46]; the mathematical expression is as follows:

$$S_{ij} = \begin{bmatrix} S_{11} & S_{12} & \cdots & S_{1n} \\ S_{21} & S_{22} & \cdots & S_{2n} \\ \vdots & \vdots & \ddots & \vdots \\ S_{n1} & S_{n2} & \cdots & S_{nn} \end{bmatrix} \tag{5}$$

where S_{ij} (km^2) is the area converted from type i to type j ($i = j$ means an area with unchanged land cover); i and j are land cover types before and after the transfer, respectively.

We established the transfer matrix of cultivated land, forest, and grassland in 2010 and 2020, and we could analyze vegetation changes by calculating the transition matrix in the past ten years.

2.3.2. Extraction of Changed Pixels

To obtain ET corresponding to different vegetation, the reference GlobalLand30 with a spatial resolution of 30 m was first re-projected to the standard MOD16A2 sinusoidal projection [47]. Then, we selected the pixels for which a total of 30 m pixel fraction for each 500 m grid was more than 60% (Figure 6a). We extracted the NDVI from points selected in different ecological subregions to verify the accuracy of the extracted vegetation types [48], and obtained NDVI features in different ecological subregions as shown in Figure 6b.

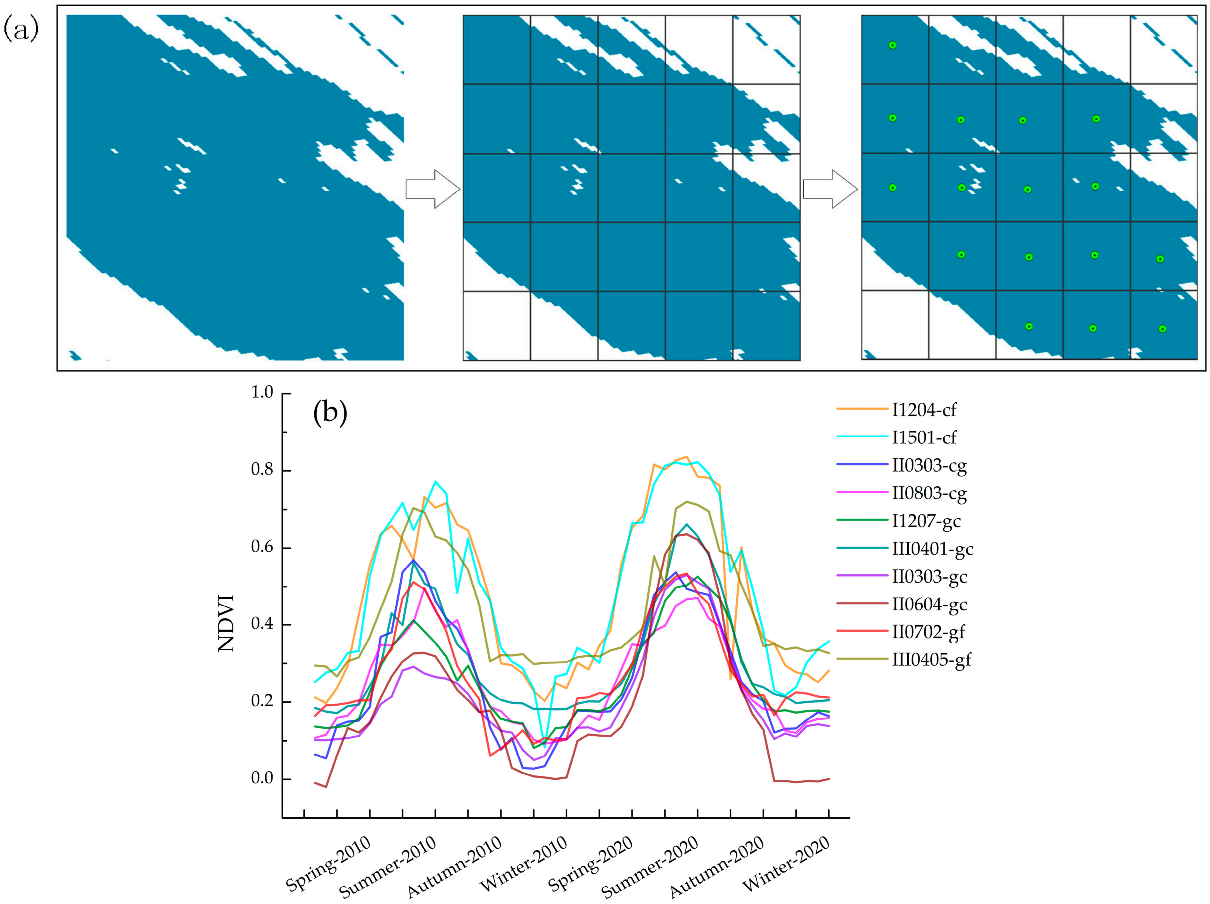

Figure 6. (**a**) Example of ~500 m grid based on 30 m pixel reference map; (**b**) features of NDVI in different subecoregions.

2.3.3. Method of Absolute Change

In this paper, inter-annual and seasonal ET differences in 2010 and 2020 are used for change analysis. The formula for calculating the absolute change is as follows:

$$Y = M_t - N_t \tag{6}$$

where Y (mm) is inter-annual variation; M_t (mm) is the ET of the spring, summer, autumn, and winter and total annual amount in 2020; and N_t (mm) is the ET of spring, summer, autumn and winter and total annual amount in 2010.

2.3.4. Method of Relative Change

ET is affected by multiple factors. Variation in ET may be also explained by warming temperatures [49]. Thus, we focused on the influence of vegetation changes on ET. In order to control a single variable, we discuss the change between the ET of vegetation changes and ET without vegetation changes; the expression is as follows:

$$Z = (ET^{i+10} - ET^{i})_{change} - (ET^{i+10} - ET^{i})_{unchange} \quad (7)$$

where Z (mm) is the relative change, ET^{i+10} (mm) is the ET of vegetation in 2020, and ET^{i} (mm) is the ET of vegetation in 2010.

To further discuss the relative change in ET, the increased ET of unchanged vegetation was taken as the reference standard to calculate the rate of relative change. The relative change value of ET after vegetation change was analyzed. The formula for calculating the relative rate of change is as follows:

$$Re = \frac{(ET^{i+10} - ET^{i})_{change} - (ET^{i+10} - ET^{i})_{unchange}}{ET^{i}_{unchange}} \quad (8)$$

where Re (%) is the relative rate of ET change, and $ET^{i}_{unchange}$ (mm) is the ET of unchanged vegetation in 2010.

3. Results and Discussion

3.1. Vegetation Changes in Northwest China

Partial changes occurred from cultivated land into forest or grassland due to returning ecological restoration, and grassland was converted into cultivated land due to food demand and security during 2010–2020. One of the dominant land cover conversion types was grassland into cultivated land. Second was the conversion from grassland into forest, and conversion from cultivated land into grassland and forest was relatively small (see Table 3).

Table 3. Transfer matrix of vegetation types from 2010 to 2020 (unit: km^2).

		2010			
		Cultivated Land	**Forest**	**Grassland**	**Total**
2020	Cultivated Land	250,149	4133	22,780	277,068
	Forest	4293	156,162	13,848	174,303
	Grassland	10,398	7927	866,321	884,645
	Total	264,839	168,222	902,949	1,336,011

We focused on analyzing vegetation changes in the following typical regions. In Northwest China, conversion from grassland into cultivated land was mainly concentrated in I1207, II0303, II0604, and III0401 because cultivated land was scientifically expanded without damaging the ecological environment due to food demand in the northwestern agricultural and pastoral transition zone, while grassland and desert kept decreasing [50]. At the same time, grassland-to-forest land conversion mainly occurred in II0702 and III0405. Cultivated land was transformed into grassland mainly in II0303 and II0803. Conversion from cultivated land into forest was mainly distributed in I1204 and I1501 because of the policy implementation of returning cultivated land to forest and grassland in Northwest China. To sum up, vegetation changes in Northwest China were mainly grassland into cultivated land, grassland into forest, cultivated land into grassland, and cultivated land into forest, and their spatial distribution characteristics are shown in Figure 7 (review no. GS (2019)1822).

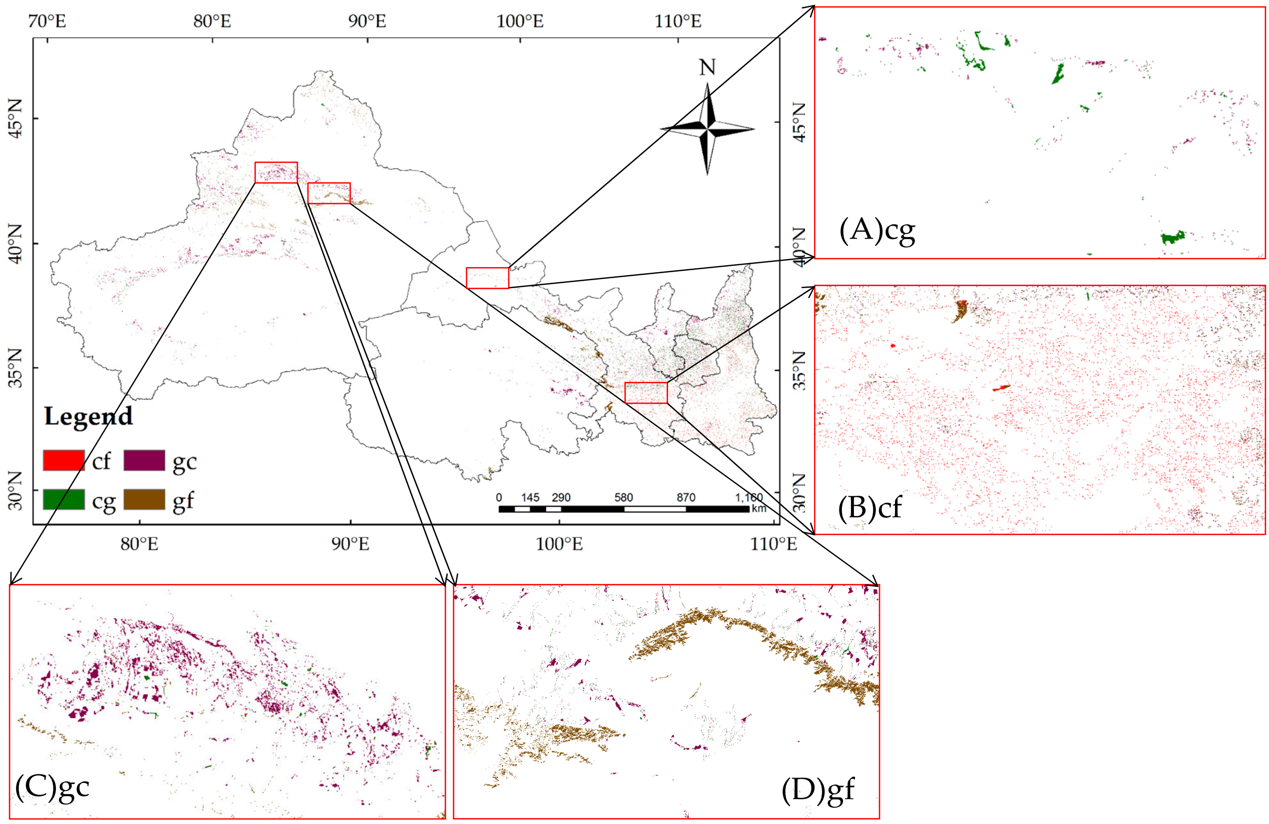

Figure 7. Spatial distribution of vegetation changes from 2010 to 2020. Note: (**B**) cf, change from cultivated land into forest; (**A**) cg, change from cultivated land into grassland, (**C**) gc, change from grassland into cultivated land; (**D**) gf change from grassland into forest.

3.2. Annual ET of Typical Vegetation in Different Regions

There are great differences in topographic and climatic conditions in each region in Northwest China. The annual ET of each vegetation type is relatively different. Therefore, we analyzed the annual ET of cultivated land and forest and grassland in each subecoregion in 2010 and 2020. ET characteristics differed significantly among different vegetation types [51]. The annual ET of cultivated land, forest, and grassland in different subecoregions is shown in Table 4. Annual ET over cultivated land was in the range of 420–520 mm, and annual ET over forests was about 600 mm in I1204 because it has a semi-humid and semi-arid climate in the western and northern part of Loess Plateau. ET generated by cultivated land was relatively the largest, annual ET was about 600 mm, while annual forest ET was about 700 mm in I1501. This is because it belongs to the humid and sub-humid climate in the south of Loess Plateau; precipitation in this region is relatively sufficient. The annual ET of cultivated land was about 400 mm, and that of grassland was about 410 mm in II0303. It has a dry climate and low rainfall, but the area is close to the Qilian Mountains, where there is meltwater from glaciers and snow, water resources are abundant, and irrigated agriculture is thus developed. The annual ET of cultivated land was less than 300 mm, approximately 240 mm, and the annual ET of grassland was about 200 mm in II0803 due to this subecoregion being extremely arid.

Table 4. Annual ET of cultivated land, grassland, and forests in different regions in 2010 and 2020.

Code	Type of Trans-formation	Annual ET of Changed Vegetation in 2010 (Mm)	Annual ET of Changed Vegetation in 2020 (Mm)	Type of Trans-formation	Annual ET of Unchanged Vegetation in 2010 (Mm)	Annual ET of Unchanged Vegetation in 2020 (Mm)
I1204	cf	516	625	cc	427	442
I1501	cf	614	688	cc	598	655
II0303	cg	424	407	cc	357	363
II0803	cg	235	204	cc	239	242
I1207	gc	384	439	gg	393	434
II0303	gc	308	345	gg	295	302
II0604	gc	221	320	gg	228	211
III0401	gc	383	441	gg	391	421
II0702	gf	339	379	gg	372	376
III0405	gf	517	627	gg	534	594

Note: cf, change from cultivated land into forest; cg, change from cultivated land into grassland; gc, change from grassland into cultivated land; gf change from grassland into forest; cc, unchanged cultivated land; gg, unchanged grassland.

The annual ET of grassland in different regions in 2010 and 2020, and annual ET converted into forest and cultivated land in 2020 are shown in Table 4. The annual ET of grassland was relatively high, between 400 and 600 mm in III0401 and III0405, the annual ET of cultivated land in III0401 was about 440 mm, and that of the forest in III0405 was about 630 mm. This is mainly because it is located in the alpine Qinghai–Tibet region, which has a continental climate on the plateau, with intense radiation and high rainfall. The annual ET of grassland in I1207 was about 400 mm, and the corresponding annual ET of cultivated land was about 440 mm. The annual ET of grassland was in the range of 200–310 mm in the arid desert–oasis agro-ecological subregion in II0303 and II0604. The annual ET of cultivated land was 320–350 mm in II0303 and II0604. The annual ET of grassland in II0702 was relatively high and could reach 340 mm, and the annual ET of the forest in this subecoregion was about 380 mm. Due to the relatively abundant rainfall and there being forest cover in the Tianshan Mountains, they have strong water conservation capacity. In conclusion, on the basis of vegetation-type analysis, the ET of cultivated land in Northwest China is greater than that of grassland in the same subecoregion, and combined with the analysis of different ecoregions, that of eastern monsoon region and arid region of Qinghai–Tibet is greater than that of the arid region on the same vegetation type.

Forests had greater water conservation capacity than that of cultivated land. However, the annual ET of forests near the Loess Plateau was 600–700 mm, and that of grassland was about 400 mm, which is comparable to the results of Schwrzel [52]; afforestation has many effects on long-term sustainable development. The annual ET of cultivated land was about 450 mm in the agricultural oasis area of the Heihe River Basin, which was similar to the research results of another study [19,53]. In general, forests are mainly distributed in the Loess Plateau, near the Tianshan Mountains in Xinjiang, and the Qilian Mountains. With the condition of sufficient water, the ET of forests was the highest, followed by cultivated land, and that of grassland was the lowest. Cultivated land was mainly distributed in the alluvial plain of the Loess Plateau and in the agricultural oasis region of the Hexi Corridor, and in the Junggar and Tarim Basins. The amount of ET produced by cultivated land is relatively large under the influence of irrigation and other human factors [54]. Because of the dry climate in Northwest China, it can achieve strong evaporation and produce a large amount of moisture with enough water, and transpiration and photosynthesis occur at the same time. When there is much loss of water, carbon sequestration is completed, organic matter is accumulated, and crop yields are improved. Compared with forests and cultivated land, the ET generated by grassland was smaller. Grassland grows in arid desert areas, and its leaves shrink in the process of continuous evolution in order to retain water and adapt to the external environment. Therefore, in terms of subecoregions in Northwest

China, for the same vegetation type, ET in the Qinghai–Tibet alpine region was much higher than that in the eastern monsoon region in Loess Plateau, and the lowest in the western arid and semi-arid region. In the same subecoregion, forest ET was higher than that of cultivated land, and the ET of grassland was relatively lower.

3.3. Effect of Typical Vegetation Changes on ET

3.3.1. Effect of Typical Vegetation Changes on Inter-annual ET

ET showed a trend of change on the basis of the vegetation change in Figure 8, and we focused on the influence of vegetation changes on ET. In order to control a single variable, the increased ET of unchanged cultivated land and unchanged grassland was taken as the reference standard. The absolute and relative change values of ET after vegetation changes were analyzed, calculated with Formulas (6)–(8).

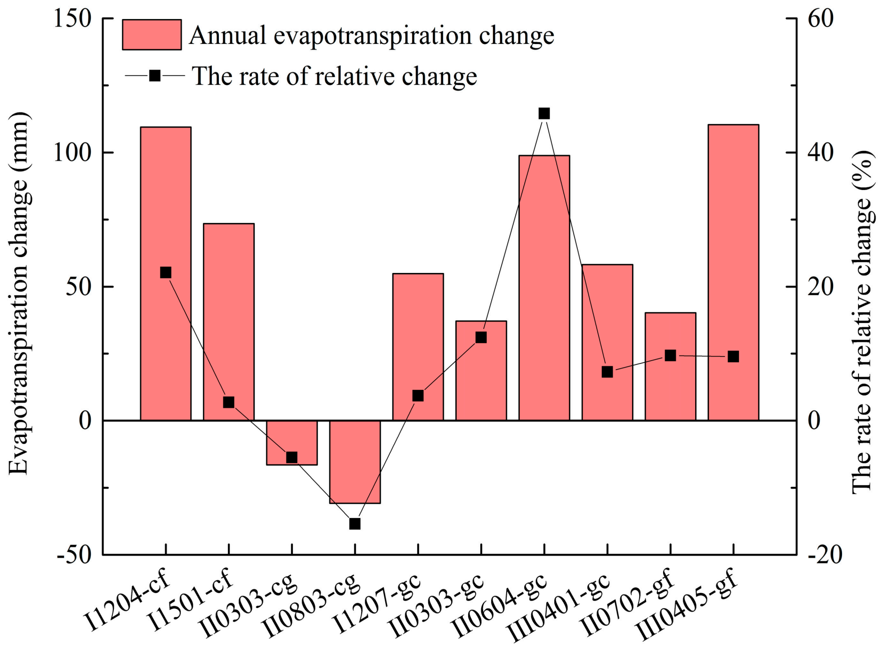

Figure 8. ET variation over typical vegetation changes from 2010 to 2020.

Afforestation and the conversion of cultivated land into forest on the Loess Plateau are very important to the water balance in the arid region [55]. With the promotion of the policy of returning sloping land into grass and planting trees, vigorously building all kinds of shelterbelts, economic forests, and artificial grasslands, and controlling soil erosion, some cultivated land was converted into forests in the Loess Plateau, the increased absolute ET was about 110 mm compared with the unchanged cultivated land, the relative rate of change increased by 22.1% after cultivated land was changed into forest in I1204; the increased absolute ET was approximately 70 mm, and the relative rate of change increased by 2.72% in I1501 (Figure 8). This was because I1204 has a sub-humid and semi-arid climate, while I1501 has a humid and semi-humid climate. ET from the conversion of cultivated land into forest in semi-humid and semi-arid regions was thus higher than that in humid and semi-humid regions.

In Northwest China, artificial licorice is vigorously developed, and desert vegetation is protected. After the conversion from cultivated land into grassland in II0303 and II0803, ET showed a decreasing trend by 16 and 25 mm, respectively. Compared with unchanged cultivated land, the relative rate of change decreased by 5.49% and 12.8%, respectively, after cultivated land had changed into grassland (Figure 8).

In order to solve the problem of food security and food demand, the area of basic cultivated land expanded in the northwestern agricultural and pastoral transition zone and other regions, as grassland in different areas was converted into cultivated land, and cultivated land expansion affects temperature extremes and thus ET [56]. As shown in Figure 8, the increase in ET in II0604 was the largest, up to 99 mm, compared with the unchanged grassland, it increased by 45.8%. The increased ET in I1207 and III0401 was between 40 and 60 mm. Because the grassland had a lower ET in II0604 in 2010, while the ET of cultivated lands was similar in I1207, II0303, II0604, and III0401 in 2020, the different value in annual ET was much larger in II0604.

After the grassland had been transformed into forest in III0405, the increased ET was approximately 110 mm compared with the unchanged grassland in this region, an increase of 9.54%; on the southern slope of Tianshan Mountain, the increased ET value was about 40 mm after the grassland had been converted into forest in II0702, a 9.71% increase compared with the unchanged grassland (Figure 8).

ET from the conversion of cultivated land into forest, grassland into cultivated land, and grassland into forest showed an increasing trend, while ET from cultivated land into grassland showed a decreasing trend. The increase in ET was the largest in II0604 after the grassland had been transformed into cultivated land, a 45.8% increase compared with that in 2010. The expansion of cultivated land should be reasonable. Excessive expansion consumes a large amount of moisture, which is not conducive to the long-term development of the ecological environment. Secondly, the rate of relative ET change increased by 22.1% after cultivated land had changed into forest in I1204. However, cultivated land was converted into forest in I1501, and the increase in ET was only 2.72% compared with that of unchanged cultivated land. To a certain extent, this can be explained by the fact that water consumption caused by converting cultivated land into forest in semi-arid and semi-humid regions was higher than that in humid and semi-humid regions. Thus, the contributions of vegetation restoration and cultivated land expansion increased ET in Northwest China [57,58].

3.3.2. Effect of Typical Vegetation Changes on Seasonal ET

We defined the seasons as spring (057–145), summer (153–241), autumn (249–329), and winter (337–049). The ET of each vegetation type is generally the highest in summer, followed by spring, autumn, and winter. The high ET in summer is due to abundant water, high temperatures, and long sunshine duration, vegetation is in a flourishing period of growth and development accompanied by transpiration and photosynthesis, and a large amount of water is emitted into the air through stomata. In spring, vegetation is in the green stage, the physiological activities of vegetation are gradually increasing, temperatures rise, ice and snow melt in all mountains, and ET shows a slight increasing trend. In autumn, vegetation gradually withers and yellows, transpiration is obviously weakened, the temperature decreases, and ET is smaller than that in spring. In winter, the physiological activity of vegetation almost stops completely, thus ET is relatively low.

The seasonal characteristics of vegetation in different regions are different and they are shown in Figure 9a–d. Figure 9a shows that, after conversion from cultivated land into forest, the increased ET in I1204 was about 28 mm in spring, 70 mm in summer, and less than that in autumn and winter. Increased ET was about 14 mm in spring, nearly 50 mm in summer, and less than that in autumn and winter in I1501. On the whole, after the conversion of cultivated land into forest, ET increased the most in the summer in the range of 50–70 mm, followed by spring in the range of 10–30 mm. ET in each season in semi-arid and semi-humid regions was higher than that in humid and semi-humid regions after the conversion of cultivated land into forest, mainly in spring and summer.

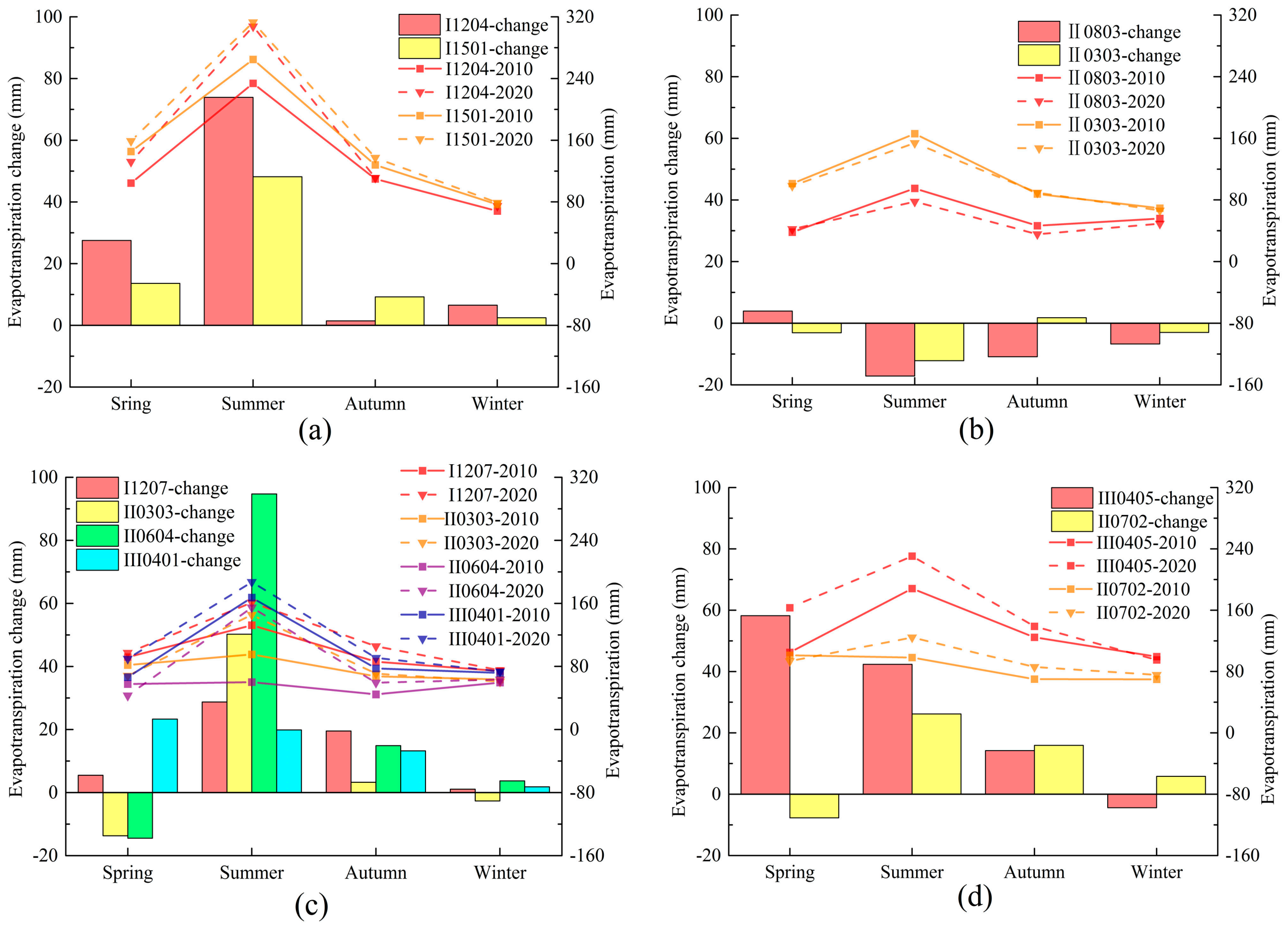

Figure 9. Seasonal variations in ET changes based on vegetation changes from 2010 to 2020. Conversion of (**a**) cultivated land into forest, (**b**) cultivated land into grassland, (**c**) grassland into cultivated land, and (**d**) grassland into forest.

Figure 9b shows that ET in II0303 and II0803 decreased after the conversion from cultivated land into grassland, mainly in summer, but the magnitude of the decrease was small. ET changed a little after the cultivated land had been changed into grassland. The decrease in ET was relatively large in summer, about 12mm, while the change in ET in other seasonal phases was less than that. The main reason was that barren cultivated land was planted with grass in order to meet animal husbandry needs.

Corresponding to Figure 9c, after conversion from grassland into cultivated land, ET increased by about 30 mm in summer, 20 mm in autumn, and less than that in spring and winter in I1207. ET increased more in summer, about 50–100 mm, and decreased by 13–15 mm in spring in II0303 and II0604. III0401 was in the dry and cold region of the Qinghai–Tibet Plateau; the ET of grassland and cultivated land had obvious seasonal characteristics, and the increased ET in spring, summer, and autumn was relatively similar, in the range of 10–25 mm.

As Figure 9d indicates, in the conversion from grassland into forest, the increased ET in II0702 was 15–30 mm in summer and autumn, and the changed ET was relatively small in spring and winter. The increased ET in spring and summer was in the range of 40–60 mm, and the changed ET in autumn and winter was relatively small in III0405.

Overall, the ET of grassland is different due to the different roots and water absorption capacity levels [59]. From the perspective of seasonal analysis, after grassland had been converted into cultivated land or forest, it was negative in spring, but positive in summer, autumn, and winter in the western arid and semi-arid region. The main reason lies in the relatively high ET of grassland in spring in areas with water supply from Tianshan and

Qilian Mountains snow melt, which contributed to the high ET of grassland in spring; thus, the grassland ET of spring and summer season phase differences was not significant, while the cultivated land was influenced by irrigation, and ET in summer was higher than that in spring, which is supported by Chen's research [60]. In the alpine Qinghai–Tibet region and the eastern monsoon Loess Plateau region, ET increased in spring, summer, autumn, and winter after grassland had been converted into cultivated land or forest.

4. Conclusions

On the basis of the GlobalLand30 land cover products in 2010 and 2020, subecoregion datasets, and temporal NDVI products, we extracted and analyzed inter-annual and seasonal MOD16A2 products, and explored the impact of typical vegetation changes in different regions of Northwest China on ET. Our conclusions are the following:

(1) In the past ten years, vegetation changes were mainly from grassland into cultivated land in the northwestern agricultural and pastoral transition zone, accompanied by the conversion of cultivated land into grassland. Then, the conversion from cultivated land into forest primarily occurred in the Loess Plateau region.

(2) There was much conversion from grassland into cultivated land in the agricultural oasis region, the maximal increased water consumption reached 99 mm/10a, and the relative rate of change increased by 45.8% compared with the unchanged grassland. ET was largely increased with an absolute magnitude value of up to 110 mm/10a, a 22.1% increase compared to that of unchanged cultivated land. However, the humid and semi-humid region of the southern Loess Plateau showed a small ET increase of about 73 mm/10a, a small relative change rate increase of 2.72%, and it would be more suitable to convert cultivated land into forest.

(3) Vegetation ET was the highest in summer, followed by spring and autumn, and with the lowest in winter. It could provide grassland with adequate water because global warming is causing the massive melting of ice and snow at the foot of mountains, and there was a small ET difference of grassland between spring and summer in arid regions. ET showed an increasing trend after cultivated land had changed into forest, and grassland had been converted into cultivated land and forest, while it showed a decreasing trend after cultivated land had changed into grassland, which was mainly manifested in the summer.

(4) Therefore, stricter policy to limit agriculture expansions should be adopted in future land use planning for sustainable ecosystem development in Northwest China. This research helps in better distinguishing ET changes from vegetation changes and managing limited water resources in future land and water allocation in arid and semiarid regions. Future work should use fine-grained vegetation classification data and the quantification of ET based on the refinement of types of cultivated land, grassland, and forest.

Author Contributions: Conceptualization, Y.S. and Y.T.; methodology, Y.T. and Y.S.; data organization, Y.T., Y.S. and C.S.; writing—original draft preparation, Y.T. and Y.S.; writing—review and editing, Y.S., Y.T., C.S., J.H., L.G., Q.Z. and R.Z.; supervision, Y.S.; funding acquisition, Y.S. All authors have read and agreed to the published version of the manuscript.

Funding: This research was supported by the National Key Research and Development Program of China (no. 2020YFA0608501), Talent recruited program of the Chinese Academy of Science (no. Y938091), National Natural Science Foundation of China (no. 42071351), the project-supporting discipline innovation team of Liaoning Technical University (no. LNTU20TD-23), and The Natural Science Foundation of Liaoning Province (no. 2020-BS-259), the Key Laboratory of Land Satellite Remote Sensing Application, Ministry of Natural Resources of the People's Republic of China (Grant no. KLSMNR-202107).

Acknowledgments: We thank the relevant teams and organizations for providing the datasets used in this study. The GlobalLand30 product was provided by the Global Geographic Information Public Product and is available at http://www.globeland30.org/, accessed on 30 December 2020. The MOD16A2 product was provided by the National Aeronautics and Space Administration, https://ladsweb.modaps.eosdis.nasa.gov/, accessed on 31 January 2021. The MOD13 A1 product was provided by the National Aeronautics and Space Administration https://ladsweb.-modaps.eosdis.

nasa.gov/, accessed on 26 May 2021. The vector of ecological data was provided by the Database of Ecological Function Region in China http://www.ecosystem.csdb.cn/ecoass/-ecoplanning.jsp, accessed on 18 March 2021.

Conflicts of Interest: The authors declare no conflict of interest.

References

1. Burman, R.; Pochop, L.O. Evaporation, evapotranspiration and climatic data. *J. Hydrol.* **1994**, *190*, 167–168.
2. Fisher, J.B.; Melton, F.; Middleton, E.; Hain, C.; Anderson, M.; Allen, R.; McCabe, M.F.; Hook, S.; Baldocchi, B.; Townsend, P.A. The future of evapotranspiration: Global requirements for ecosystem functioning, carbon and climate feedbacks, agricultural management, and water resources. *Water Resour. Res.* **2017**, *53*, 2618–2626. [CrossRef]
3. Wang, K.C.; Dickinson, R.E. A review of global terrestrial evapotranspiration: Observation, modeling, climatology, and climatic variability. *Rev. Geophys.* **2012**, *50*, RG2005. [CrossRef]
4. Li, C.J.; Hu, S.J.; Zheng, B.W. Energy balance and evapotranspiration characteristics of Haloxylon ammodendron community in the southern margin of the Gurbantunggut Desert. *Acta Ecol. Sin.* **2021**, *41*, 92–100.
5. Ma, X.H.; Feng, Q. Energy partitioning and evapotranspiration of Populus euphratica forests in desert riparian area. *Acta Ecol. Sin.* **2020**, *40*, 8683–8693.
6. Zhou, S.; Williams, A.P.; Lintner, B.R.; Berg, A.M.; Zhang, Y.; Keenan, T.F.; Cook, B.I.; Hagemann, S.; Seneviratne, A.I.; Gentine, P. Soil moisture–atmosphere feedbacks mitigate declining water availability in drylands. *Nat. Clim. Chang.* **2021**, *11*, 38–44. [CrossRef]
7. Tang, R.; Zhao, Y.T.; Lin, H.L. Spatio-Temporal Variation Characteristics of Aboveground Biomass in the Headwater of the Yellow River Based on Machine Learning. *Remote Sens.* **2021**, *13*, 3404. [CrossRef]
8. Arellano, J.V.; Heerwaarden, C.C.; Lelieveld, J. Modelled suppression of boundary-layer clouds by plants in a CO_2-rich atmosphere. *Nat. Geosci.* **2012**, *5*, 701–704. [CrossRef]
9. Hu, Z.M.; Wu, G.N.; Zhang, L.X.; Li, S.G.; Zhu, X.J.; Zheng, H.; Zhang, L.M.; Sun, X.M.; Yu, G.R. Modeling and Partitioning of Regional Evapotranspiration Using a Satellite-Driven Water-Carbon Coupling Model. *Remote Sens.* **2017**, *9*, 54. [CrossRef]
10. Ptichnikov, A.V.; Shvarts, E.A.; Kuznetsova, D.A. The Greenhouse Gas Absorption Potential of Russian Forests and Possibilities for Carbon Footprint Reduction for Exported Domestic Products. *Dokl. Earth Sci.* **2021**, *499*, 683–685. [CrossRef]
11. Miller, B.A.; Pearse, W.D.; Flint, C.G. Saving the Forest from the Trees: Expert Views on Funding Restoration of Northern Arizona Ponderosa Pine Forests through Registered Carbon Offsets. *Forests* **2021**, *12*, 1119. [CrossRef]
12. Zhu, Z.C.; Piao, S.L.; Myneni, R.B.; Huang, M.T.; Zeng, Z.Z.; Canadell, J.G.; Ciais, P.; Sitch, P.; Arneth, A.; Cao, C.X. Greening of the Earth and its drivers. *Nat. Clim. Chang.* **2016**, *6*, 791–795. [CrossRef]
13. Liu, M.; Tang, R.L.; Li, Z.L.; Gao, M.F.; Yao, Y.J. Progress of data-driven remotely sensed retrieval methodsand products on land surface evapotranspiration. *Natl. Remote Sens. Bull.* **2021**, *25*, 1517–1537.
14. Running, S.; Mu, Q.Z. University of Montana and MODAPS SIPS—NASA. In MOD16A2 MODIS/Terra Evapotranspiration 8-day L4 Global 500m SIN Grid. *NASA LP DAAC* **2015**. [CrossRef]
15. Mu, Q.Z.; Heinsch, F.A.; Zhao, M.S.; Running, S.W. Development of a global evapotranspiration algorithm based on MODIS and global meteorology data. *Remote Sens. Environ.* **2007**, *111*, 519–536. [CrossRef]
16. Mu, Q.Z.; Zhao, M.S.; Running, S.W. Improvements to a MODIS global terrestrial evapotranspiration algorithm. *Remote Sens. Environ.* **2011**, *115*, 1781–1800. [CrossRef]
17. Liang, S.L.; Cheng, J.; Jia, K.; Jiang, B.; Liu, Q.; Xiao, Z.Q.; Yao, Y.J.; Yuan, W.P.; Zhang, X.T.; Zhao, X.; et al. The Global Land Surface Satellite (GLASS) product suite. *Bull. Am. Meteorol. Soc.* **2021**, *102*, E323–E337. [CrossRef]
18. Jung, M.; Reichstein, M.; Margolis, H.A.; Cescatti, A.; Richardson, A.D.; Arain, M.A.; Arneth, A.; Bernhofer, C.; Bonal, D.; Chen, J.; et al. Global patterns of land-atmosphere fluxes of carbon dioxide, latent heat, and sensible heat derived from eddy covariance, satellite, and meteorological observations. *J. Geophys. Res.* **2011**, *116*, G00J07. [CrossRef]
19. Hu, G.C.; Jia, L. Monitoring of Evapotranspiration in a Semi-Arid Inland River Basin by Combining Microwave and Optical Remote Sensing Observations. *Remote Sens.* **2015**, *7*, 3056–3087. [CrossRef]
20. Wu, B.F.; Yan, N.N.; Xiong, J.; Bastiaanssen, W.G.M.; Zhu, W.W.; Stein, A. Validation of ETWatch using field measurements at diverse landscapes: A case study in Hai Basin of China. *J. Hydrol.* **2012**, *436–437*, 67–80. [CrossRef]
21. He, T.; Shao, Q.Q. Temporal and spatial patterns of Evapotranspiration in China from 2001 to 2010 based on MOD16 products. *J. Geo-Inf. Sci.* **2014**, *16*, 979–988.
22. Cai, D.; Ge, Q.; Wang, X.; Liu, B.; Goudie, A.S.; Hu, S. Contributions of ecological programs to vegetation restoration in arid and semiarid China. *Environ. Res. Lett.* **2020**, *15*, 114046. [CrossRef]
23. Liu, J.Y.; Ning, J.; Kuang, W.H.; Xu, X.L.; Zhang, S.W.; Yan, Z.Z.; Li, R.D.; Wu, S.X.; Hu, Y.F.; Du, G.M.; et al. Spatio-temporal patterns and characteristics of land-use change in China during 2010–2015. *Acta Geogr. Sin.* **2018**, *73*, 5–8.
24. Cheng, W.M.; Gao, X.Y.; Ma, T.; Xu, X.L.; Chen, Y.J.; Zhou, C.H. Spatial-temporal distribution of cropland in China based on geomorphologic regionalization during 1990–2015. *Acta Geogr. Sin.* **2018**, *73*, 1613–1629.
25. Deng, X.; Shi, Q.; Zhang, Q.; Shi, C.; Yin, F. Impacts of land use and land cover changes on surface energy and water balance in the Heihe River Basin of China, 2000–2010. *Phys. Chem. Earth* **2015**, *79*, 2–10. [CrossRef]

26. Chen, Y.L.; Wang, S.S.; Ren, Z.G.; Huang, X.Z.; Liu, S.S.; Deng, H.J.; Lin, W.K. Increased evapotranspiration from land cover changes intensified water crisis in an arid river basin in northwest China. *J. Hydrol.* **2019**, *574*, 383–397. [CrossRef]
27. Qiu, L.J.; Wu, Y.P.; Shi, Z.Y.; Chen, Y.T.; Zhao, F.B. Quantifying the Responses of Evapotranspiration and Its Components to Vegetation Restoration and Climate Change on the Loess Plateau of China. *Remote Sens.* **2021**, *13*, 2358. [CrossRef]
28. Qiu, L.J.; Wu, Y.P.; Shi, Z.Y.; Yu, M.; Zhao, F.B.; Guan, Y.H. Quantifying spatiotemporal variations in soil moisture driven by vegetation restoration on the Loess Plateau of China. *J. Hydrol.* **2021**, *600*, 126580. [CrossRef]
29. Jiang, F.X.; Xie, X.H.; Liang, S.L.; Wang, Y.B.; Zhu, B.W.; Zhang, X.T.; Chen, Y.C. Loess Plateau evapotranspiration intensified by land surface radiative forcing associated with ecological restoration. *Agric. For. Meteorol.* **2021**, *311*, 108669. [CrossRef]
30. Piao, S.L.; Nan, H.J.; Huntingford, C.; Ciais, P.; Friedlingstein, P.; Sitch, S.; Peng, S.S.; Ahlström, A.; Canadell, J.G. Evidence for a weakening relationship between interannual temperature variability and northern vegetation activity. *Nat. Commun.* **2014**, *5*, 5018. [CrossRef]
31. Wang, H.H.; Zhao, J.; Yue, C.; Yu, Q. Cooling effect induced by afforestation on the loess plateau and its change law. *J. Soil Water Conserv.* **2021**, *35*, 214–220.
32. Shuai, Y.M.; Masek, J.G.; Gao, F.; Schaaf, C.B.; He, T. An approach for the long-term 30-m land surface snow-free albedo retrieval from historic Landsat surface reflectance and MODIS-based a priori anisotropy knowledge. *Remote Sens. Environ.* **2014**, *152*, 467–479. [CrossRef]
33. Gu, J.H.; Xue, H.Z.; Dong, G.T.; Zhou, L.J.; Li, J.R.; Dang, S.Z.; Li, S.Z. Effects of NDVI/ land use on spatial-temporal variation of Evapotranspiration in the Yellow River Basin. *Arid. Land Geogr.* **2021**, *44*, 158–167.
34. Cui, Y.K.; Jia, L.; Fan, W.J. Estimation of actual evapotranspiration and its components in an irrigated area by integrating the Shuttleworth-Wallace and surface temperature-vegetation index schemes using the particle swarm optimization algorithm. *Agric. For. Meteorol.* **2021**, *307*, 108488. [CrossRef]
35. Noormets, A.; Bracho, R.; Ward, E.; Seiler, J.; Strahm, B.; Lin, W.; McElligott, K.; Domec, J.C.; GonzalezBenecke, C.; Jokela, E.J. Heterotrophic respiration and the divergence of productivity and carbon sequestration. *Geophys. Res. Lett.* **2021**, *48*, e2020GL092366. [CrossRef]
36. Chen, J.; Chen, J.; Gong, P.; Liao, A.P.; He, C.Y. Higher Resolution Global Land Cover Mapping. *Geomat. World* **2011**, *9*, 12–14.
37. Chen, J.; Chen, J.; Lia, A.P.; Cao, X.; Chen, L.J.; Chen, X.H.; Peng, S.; Han, G.; Zhang, H.W.; He, C.Y. Concepts and key techniques for 30m global land cover mapping. *Acta Geod. Cartogr. Sin.* **2014**, *43*, 551–557.
38. Chen, J.; Chen, J.; Liao, A.P.; Cao, X.; Chen, L.J.; Chen, X.H.; He, C.Y.; Han, G.; Peng, S.; Lu, M. Globalland cover mapping at 30 m resolution: A POK-based operational approach. *ISPRS J. Photogramm.* **2015**, *103*, 7–27. [CrossRef]
39. Zhao, J.F.; Li, C.; Yang, T.Y.; Tang, Y.H.; Yin, Y.L.; Luan, X.B.; Sun, S.K. Estimation of high spatiotemporal resolution actual evapotranspiration by combining the SWH model with the METRIC model. *J. Hydrol.* **2020**, *586*, 124883. [CrossRef]
40. He, L.; Chen, J.M.; Chen, J.; Liu, J.; Rogers, C.A. Diverse photosynthetic capacity of global ecosystems mapped by satellite chlorophyll fluorescence measurements. *Remote Sens. Environ.* **2019**, *232*, 111344. [CrossRef]
41. Chen, J.M.; Liu, J. Evolution of evapotranspiration models using thermal and shortwave remote sensing data. *Remote Sens. Environ.* **2020**, *237*, 111594. [CrossRef]
42. Yuan, W.P.; Zheng, Y.; Piao, S.L.; Ciais, P.; Lombardozzi, D.; Wang, Y.P.; Ryu, Y.; Chen, G.X.; Dong, W.J.; Hu, Z.M. Increased atmospheric vapor pressure deficit reduces global vegetation growth. *Sci. Adv.* **2019**, *5*, eaax1396. [CrossRef] [PubMed]
43. Vanderhoof, M.K.; Williams, C.A. Persistence of MODIS evapotranspiration impacts from mountain pine beetle outbreaks in lodgepole pine forests, south-central Rocky Mountains. *Agric. For. Meteorol.* **2015**, *200*, 78–91. [CrossRef]
44. Kamel, D. University of Arizona, Alfredo Huete—University of Technology Sydney and MODAPS SIPS—NASA. In MOD13A1 MODIS/Terra Vegetation Indices 16-Day L3 Global 500m SIN Grid. *NASA LP DAAC* **2015**. [CrossRef]
45. Rouse, J.W.; Haas, R.W.; Schell, J.A.; Deering, D.W.; Harlan, J.C. Monitoring the vernal advancement and retrogradation (green wave effect) of natural vegetation. *NASA/GSFC Type III Final. Rep. Greenbelt. Md.* **1974**, *371*, 1–112.
46. Zhu, H.Y.; Li, X.B. Discussion on the Index Method of Regional Land Use Change. *Acta Geogr. Sin.* **2003**, *58*, 643–650.
47. Hu, Q.; Ma, Y.X.; Xu, B.D.; Song, Q.; Tang, H.J.; Wu, W.B. Estimating Sub-Pixel Soybean Fraction from Time-Series MODIS Data Using an Optimized Geographically Weighted Regression Model. *Remote Sens.* **2018**, *10*, 491. [CrossRef]
48. Wang, H.J.; Li, Z.; Cao, L.; Feng, R.; Pan, Y.P. Response of NDVI of Natural Vegetation to Climate Changes and Drought in China. *Land* **2021**, *10*, 966. [CrossRef]
49. Pascolini-Campbell, M.; Reager, J.T.; Chandanpurkar, H.A.; Rodell, M. A 10 percent increase in global land evapotranspiration from 2003 to 2019. *Nature* **2021**, *593*, 543–547. [CrossRef]
50. Yuan, C.C.; Zhang, D.X.; Liu, L.M.; Ye, J.W. Regional characteristics and spatial-temporal distribution of cultivated land change in China during 2009–2018. *Trans. CSAE* **2021**, *37*, 267–278.
51. Wu, R.J.; Xing, X.R. Variation characteristics and influencing factors of actual evapotranspiration under various vegetation types: Acase study in the Huaihe River Basin, China. *Chin. J. Appl. Ecol.* **2016**, *27*, 1727–1736.
52. Schwrzel, K.; Zhang, L.L.; Montanarella, L.; Wang, Y.H.; Sun, G. How afforestation affects the water cycle in drylands: A process-based comparative analysis. *Glob. Chang. Biol.* **2020**, *26*, 944–959. [CrossRef] [PubMed]
53. Wang, W.Z.; Xu, F.N.; Wang, J.M. Energy Exchange and Evapotranspiration over the Ejina Oasis Riparian Forest Ecosystem with Different Land-Cover Types. *Water* **2021**, *13*, 3424. [CrossRef]

54. Yan, J.X.; Ma, Y.F.; Zhang, D.Y.; Li, Z.C.; Zhang, W.K.; Wu, Z.H.; Wang, H.; Wen, L.H. High-Resolution Monitoring and Assessment of Evapotranspiration and Gross Primary Production Using Remote Sensing in a Typical Arid Region. *Land* **2021**, *10*, 396. [CrossRef]
55. Zhang, Y.K.; Huang, M.B. Spatial variability and temporal stability of actual evapotranspiration on a hillslope of the Chinese Loess Plateau. *J. Arid. Land* **2021**, *13*, 189–204. [CrossRef]
56. Liu, J.X.; Shen, W.H.; He, Y.Q. Effects of Cropland Expansion on Temperature Extremes in Western India from 1982 to 2015. *Land* **2021**, *10*, 489. [CrossRef]
57. Yuan, X.L.; Bai, J.; Li, L.H.; Alishir, K.; Philippe, D.M.; Hui, D. The dominant role of climate change in determining changes in evapotranspiration in Xinjiang, china from 2001 to 2012. *PLoS ONE* **2017**, *12*, e0183071. [CrossRef]
58. Wang, S.; Cui, C.F.; Dai, Q. Contributions of Vegetation Greening and Climate Change to Evapotranspiration Trend after Large-Scale Vegetation Restoration on the Loess Plateau, China. *Water* **2021**, *13*, 1755. [CrossRef]
59. Hu, H.Y.; Zhu, L.; Li, H.X.; Xu, D.M.; Xie, Y.Z. Seasonal changes in the water-use strategies of three herbaceous species in a native desert steppe of Ningxia, China. *J. Arid. Land* **2021**, *13*, 109–112. [CrossRef]
60. Chen, X. *Retrieval and Analysis of Evapotranspiration in Central Areas of Asia*; Meteorological Press: Beijing, China, 2012; pp. 182–202.